Multi-pinhole SPECT Calibration: Influence of Data Noise and Systematic Deviation

Lin Zhou, Kathleen Vunckx and Johan Nuyts

***Abstract*—Previously it has been proved that the geometry of a multi-pinhole SPECT system with circular orbit can be uniquely determined from a measurement of two point sources, without the knowledge of the distance between them. In this paper, we report that this conclusion only holds if the motion of the camera is perfectly circular. In reality, the detector heads systematically slightly deviate from the circular orbit, which may introduce non-negligible bias in the calibrated parameters. An analytical linear model was extended to estimate the influence of both data noise and systematic deviations on the accuracy of the calibration and the image quality of the reconstruction. It turns out that applying the knowledge of the distances greatly reduces the reconstruction error, especially in the presence of systematic deviations. In addition, we propose that instead of using the information about the distances between the point sources, it is more straightforward to use the knowledge about the distances between the pinhole apertures during multi-pinhole calibration. The two distance-fixing approaches yield similar calibration accuracy, but fixing the inter-pinhole distances is more preferable since it facilitates simultaneous animal-calibration data acquisition. Our theoretical results are supported by reconstruction images of a Jaszczak-type phantom.**

I. Introduction

For small animal single photon emission computed tomography (SPECT), geometrical calibration is often needed to obtain an accurate description of the system geometry. In [1], [2], it has been proved mathematically that for a multi-pinhole SPECT system, we only need two radioactive point sources to have a unique solution of calibration, without using the distance information between the two points. However, our preliminary tests with measured data indicated that if the distance between the point sources is not fixed, the calibration of the multi-pinhole system may be unstable and the dimension of the reconstruction may suffer from a large scaling effect.

Actually, one of the assumptions in [1], [2] is that the gamma camera follows a perfect circular motion during the acquisition. In reality, there are always slight deviations between the circular orbit and the actual orbit due to gravity, mechanical imprecisions, or other reasons [3], [4]. For each acquisition position, the ensemble of the detector and the pinhole collimator can be considered as a rigid object subject to 6 degrees of freedom, including small translations and rotations in 3 directions. In general we call these *systematic deviations* in the context of this paper. The systematic deviations will introduce bias on the calibration results if one assumes perfect camera motion during the calibration. However, since the deviations are expected to be very small, the bias was assumed to be negligible in the previous studies.

In this study, we extend an analytical linear approximation model, which was previously used to estimate the noise propagation property in single pinhole calibration [5], to investigate the influence of data noise and systematic deviations on the multi-pinhole calibration result. The procedure first estimates the bias and variance on the estimated parameters (calibration accuracy), and uses these to predict the resolution loss and image deformation in the reconstructed images (reconstruction accuracy). With this method, the stability and accuracy of the calibration result with and without the prior knowledge of the distance are further explored. Furthermore, we propose that for multi-pinhole calibration, it is more straightforward to extract the distance information from pinhole positions rather than from point source locations due to practical considerations.

II. Method

A. Principle of Calibration

1) Calibration Procedure: To perform a geometric calibration, normally we put N radioactive point sources (in our case N = 3) in the center of the field of view (FOV) of the pinhole collimator, and acquire the data using the same geometry and same protocol as the animal/phantom scan. Initial values are given to all the geometrical parameters and the point sources locations. With the initial estimates, we can calculate the coordinates of the point source projections. All the parameters are then fitted by comparing the estimated projections to the mass centers of the measured point projections using a penalized least square fitting procedure [6].

2) Distance as Prior Information: In order to increase the robustness of the calibration result, we always use the knowledge about the distances between the point sources during the calibration. For 3 point sources, it is achieved by transforming the Cartesian coordinates of the point sources into 3 translations, 3 rotations and 3 distances. For 2 point sources, one obtains 3 translations, 2 rotations and 1 distance. The distances describe the configuration of the rigid calibration phantom. The translations and rotations describe the specific position of the calibration phantom in the FOV. Therefore, if we have a rigid calibration phantom with known inter-point distance(s), only the translations and rotations need to be estimated to determine the point source positions.

Similar to the calibration phantom, the configuration of our multi-pinhole plate is also rigid. Therefore we can apply the same approach to use the inter-pinhole distances as prior information. Taking the pinhole offsets and the pinhole-to-detector distance as Cartesian coordinates to denote the

The authors are with the Dept. of Nuclear Medicine, K.U.Leuven, B-3000 Leuven, Belgium.

This work is supported by F.W.O. grant G.0569.08, by IUAP grant - NIMI, by EC and by IMIR project of K.U.Leuven.

pinhole position, the coordinate transformation will end up with 3 translations, 3 rotations and $3 \times (I-2)$ distances, with I the number of pinholes ($I \geq 3$). Once these distances are accurately known, we can fix them and only estimate the translations and rotations during the calibration.

B. Calibration Accuracy

We use P to denote the unknown parameter set that needs to be estimated, which consists of both camera-specific parameters and point source locations. We use U_0 to denote the ideal projection coordinates and U as the projection coordinates which are disturbed by either the measured noise or by systematic deviations. The difference is thus $\Delta U = U - U_0$. We assume

$$\Delta U = M \Delta P \tag{1}$$

where ΔP is a column matrix with the small variations in the unknown parameters P, and M is a matrix containing the first-order derivatives of the projection coordinates U_0 to each parameter of P.

The least squares solution of the linear system of (1) yields

$$\Delta P = (M^T M)^{-1} M^T \Delta U \tag{2}$$

We will use Eq. (2) to estimate the variance and the bias on the calibrated parameter P, due to data noise and systematic deviations, respectively.

If the projection coordinates U are only disturbed by zero mean Gaussian noise, the noise is characterized by its covariance matrix $\mathrm{Cov}(U)$. The calibration accuracy can then be expressed by the covariance matrix of P:

$$\mathrm{Cov}(P) = (M^T M)^{-1} M^T \mathrm{Cov}(U) M (M^T M)^{-1} \tag{3}$$

The variances on the parameters are the diagonal elements of the covariance matrix.

If the projection coordinates U are subject to systematic deviations, we represent the deviations as ΔU, and then Eq. (2) provides ΔP representing in this case the bias on the estimated parameters.

C. Reconstruction Accuracy

To evaluate the quality of the reconstruction image, we need figures of merit for the loss in the spatial resolution and the image deformation. They are calculated by analytically reconstructing a grid of points which is considered sufficiently covering the field of view of the multi-pinhole system. For a point on the grid $X_q = [x_q, y_q, z_q]$, the projection rays that go through this point can be generally written as

$$A_q X_q + B_q = 0 \tag{4}$$

With noise or systematic deviations on the data, we have a calibration error (variance or bias) in the result, introducing small variations in the estimated parameters. This yields matrices ${A'}_q$ and ${B'}_q$. As a result, Eq. (4) is typically overdetermined. In this case, we estimated the coordinates of the 'reconstructed' point source X_q^R as the least squares solution of the linear equation Eq. (4):

$$X_q^R = -({A'}_q^T {A'}_q)^{-1} {A'}_q^T {B'}_q \tag{5}$$

The loss of spatial resolution is estimated based on the distance (denoted by $S_{iq}(\theta)$) between the reconstructed point $X_q^R = [x_q^R, y_q^R, z_q^R]$ and the corresponding back-projection ray through the i-th pinhole aperture along angle θ. At each projection angle θ, we decompose S_{iq} in three directions as $S_{iq} = [s_{iq}^x, s_{iq}^y, s_{iq}^z]$, and take the longest length among all three dimensions, all acquisition angles and all points on the grid with back-projection rays through all pinhole apertures as the measure of the resolution loss.

$$\text{Res. Loss} = \max_i(\max_q(\max_\theta(\max_\epsilon(\|s_{iq}^\epsilon(\theta)\|)))) \tag{6}$$

where $\epsilon \in (x, y, z)$ indicates the direction of the measure and $\|\cdot\|$ represents the Euclidean norm.

The image deformation is evaluated from the relative difference in the distance between any two points on the grid before and after the reconstruction. Let p and q be the index of the two points, the corresponding relative difference T_{pq} is defined as

$$T_{pq} = \frac{\|X_p^R - X_q^R\| - \|X_p - X_q\|}{\|X_p - X_q\|} \times 100\% \tag{7}$$

We take the maximal value of T_{pq} among all points combinations on the grid as the image deformation.

$$\text{Img. Def.} = \max_p(\max_q(\|T_{pq}\|)) \tag{8}$$

D. Truncation Modeling

In reality, a point source will not always be detected through every pinhole aperture at every projection angle. This data truncation is modeled by only preserving the columns or rows in U, M and cov(U) corresponding to those projection points that are located in the FOV of the aperture and in the valid detector area.

III. Studies

The studies were performed with both the proposed analytical method and real measurement, based on our self-designed 7-pinhole collimators [7] for a typical acquisition setting. The calibration phantom in use was a Bequé phantom [5] which consists of three radioactive point sources (see Fig. 2, top left). The data was acquired at 64 projection angles equally spread over 360°.

We used four different calibration methods:

- fitting all parameters, including all distances,
- fixing only the inter-point distance(s),
- fixing only the inter-pinhole distances,
- fixing both the inter-point and inter-pinhole distances.

combined with three point source settings (see Fig. 2, left):

- projection data of all 3 point sources,
- projection data of the 1st and the 2nd point source,
- projection data of the 1st and the 3rd point source

which are referred to as *3PS*, *2PS-sub12* and *2PS-sub13*, respectively.

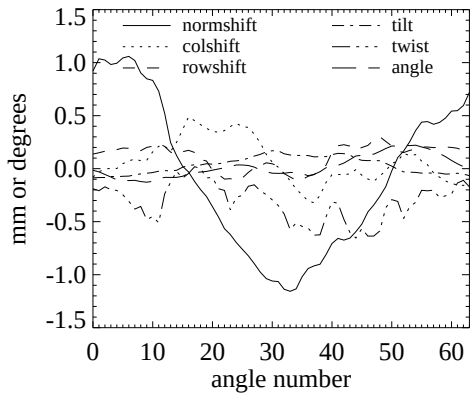

Fig. 1. Plot of systematic deviations (translations and rotations of the detector head) acquired from previously acquired calibration data. Different line types represent different degrees of freedom. The translations are expressed in mm, the rotations in degrees.

A. Analytical Evaluation

For the analytical study, the detector distance and the focal length of the pinhole collimator were chosen to be 206 mm and 176 mm, respectively. The electrical shifts, tilt angle and twist angle were set to zero. The calibration phantom was positioned in the center of the field of view. The inter-point distances were 26 mm, 19 mm and 26 mm, respectively.

The proposed analytical linear model was applied to evaluate the reconstruction accuracy of different calibration methods combined with different point source settings. The influence of both noise and systematic deviations were investigated. The error on the determination of the centroid of the projection points due to noise was modeled by a Gaussian distribution with a standard deviation of 0.6 mm. The systematic deviations used were estimated from a previous calibration procedure. The deviation patterns of all 6 degrees of freedom are plotted in Fig. 1.

The grid of points used to evaluate the reconstruction accuracy consists of two semi-circles that have a radius of 10 mm and 20 mm, respectively. To model the truncation, the truncated point projections due to the limited FOV of each pinhole were removed using a mask generated based on the measured sensitivity of that pinhole aperture.

The analytical results were verified by numerical simulations with 100 noise realizations.

B. Jaszczak Phantom Reconstruction

To visually inspect the influence of calibration errors, we reconstructed a Jaszczak-type phantom using the calibrated parameters obtained from different calibration approaches. The Jaszczak-type phantom consists of 6 sets of hollow rods having a diameter ranging from 1.5 mm to 3.0 mm in steps of 0.3 mm. The phantom was filled with 37 MBq ^{99m}Tc and scanned on a clinical gamma camera equipped with our self-designed multi-pinhole collimator. The calibration data were acquired immediately after the phantom scan. The three point sources were filled with 1.85 MBq ^{99m}Tc each and were scanned using the same geometry.

The dimension of the reconstruction image was $72\times72\times88$ with 0.6^3 mm^3 voxel. The ordered subset expectation maximization (OSEM) [8] algorithm was used for reconstruction. Corrections for decay and scatter were applied, attenuation was ignored.

IV. Results

A. Analytical Evaluation

In Table I, we list the resolution loss and image deformation, due to data noise and systematic deviations, respectively. The figures between the brackets are the corresponding values acquired from numerical simulations presented for validation purpose. In most of the cases the reconstruction accuracies predicted by our linear approximation model are in good agreement with those obtained from simulations.

We can see that, first, with the given systematic deviations, the reconstruction errors due to noise are negligible compared with those due to bias. Second, regardless of the cause of the error, the reconstruction accuracy (especially the image deformation) always improves if we applied the prior knowledge of either the inter-point or inter-pinhole distances during the calibration. Third, the reconstruction image will suffer from very large image deformation if no distance is fixed. This deformation results in a reduction of the object dimensions by 15-30$\%$. Fourth, with the given point source position, the 2PS-sub12 leads to similar resolution accuracy as 3PS, whereas 2PS-sub13 results in very bad resolution in the reconstruction.

B. Jaszczak Phantom Reconstruction

Fig. 2 shows trans-axial slices of the reconstruction images of the Jaszczak phantom. If no distance is fixed during the calibration, the reconstruction image is obviously scaled. However, once we fix either inter-point or inter-pinhole distances, the deformation becomes negligible. The resolution with 2PS-sub12 is comparable with that of 3PS. The resolution with 2PS-sub13 is however much worse. These findings are all in accordance with Table I.

V. Conclusion

In this study, we extended an analytical linear approximation model to investigate the influence of data noise and systematic deviations on multi-pinhole calibration. We use this method to estimate the bias and variance on each geometrical parameter (calibration accuracy), as well as the resolution loss and image deformation in the reconstructed image (reconstruction accuracy). Results show that the reconstruction errors are dominated by small systematic deviations from the camera orbit, rather than by noise on the estimated coordinates of the point source projections. It is also shown that if no prior knowledge about any distance is applied, the dimension of the reconstruction image may be considerably scaled due to biased parameters. The two distance-fixing methods yield similar calibration accuracy, but fixing the inter-pinhole distances is more preferable since it facilitates simultaneous animal-calibration data acquisition. The resolution loss in the reconstructed images can be significantly reduced by carefully positioning the point sources, and it is possible to obtain similar results with 2 and 3 point sources.

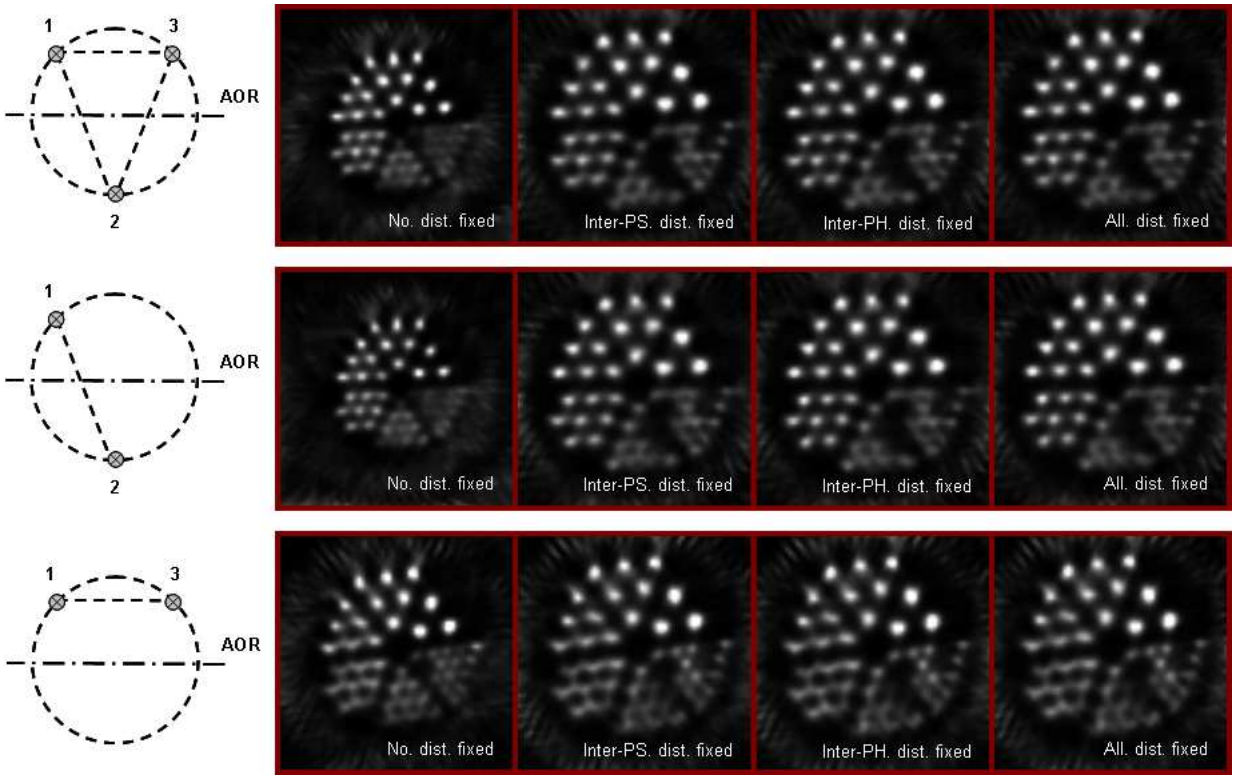

Fig. 2. Trans-axial slices of Jaszczak phantom reconstructions. Top / middle / bottom group: with 3PS / 2PS-sub12 / 2PS-sub13 calibration setting. Left to right in each group: with four different calibration methods (No distance fixed, inter-point distance(s) fixed, inter-pinhole distances fixed and all distances fixed).

TABLE I
RECONSTRUCTION ACCURACY (TRUNCATED PROJECTIONS)

	3PS		2PS-sub12		2PS-sub13	
Due to data noise	Res. Loss	Img. Def.	Res. Loss	Img. Def.	Res. Loss	Img. Def.
No distances fixed	0.029 (0.028)	0.772% (0.822%)	0.034 (0.033)	1.129% (1.105%)	0.038 (0.035)	0.873% (0.920%)
Inter-point distance(s) fixed	0.026 (0.026)	0.054% (0.056%)	0.030 (0.033)	0.133% (0.122%)	0.037 (0.039)	0.086% (0.081%)
Inter-pinhole distances fixed	0.012 (0.013)	0.056% (0.061%)	0.022 (0.021)	0.113% (0.103%)	0.016 (0.016)	0.058% (0.057%)
All distances fixed	0.012 (0.012)	0.042% (0.042%)	0.022 (0.023)	0.113% (0.112%)	0.016 (0.016)	0.057% (0.055%)
Due to systematic deviations	Res. Loss	Img. Def.	Res. Loss	Img. Def.	Res. Loss	Img. Def.
No distances fixed	1.01 (0.78)	-25.5% (-27.0%)	0.97 (0.78)	-31.1% (-30.9%)	2.28 (1.95)	-15.4% (-16.8%)
Inter-point distance(s) fixed	0.74 (0.75)	1.42% (1.41%)	0.73 (0.74)	-3.43% (-3.68%)	2.21 (2.18)	2.33% (1.76%)
Inter-pinhole distances fixed	0.84 (0.83)	1.51% (1.41%)	0.71 (0.72)	-3.09% (-3.43%)	2.30 (2.29)	2.21% (1.62%)
All distances fixed	0.79 (0.80)	1.34% (1.31%)	0.71 (0.72)	-3.09% (-3.43%)	2.29 (2.28)	2.20% (1.61%)

REFERENCES

[1] Y. C. Wang and B. M. W. Tsui, "Pinhole SPECT with different data acquisition geometries: Usefulness of unified projection operators in homogeneous coordinates." *IEEE Trans. Med. Imag.*, vol. 26(3), pp. 298-308, 2007.

[2] K. Vunckx, M. Defrise, D. Bequé, C. Vanhove, A. Andreyev, and J. Nuyts, "Geometrical calibration and aperture configuration design in multi-pinhole SPECT." *IEEE Internat. Symp. on Biomed. Imag.*, pp. 1403-1406, 2008.

[3] S. D. Metzler and N. H. Patil, "Measuring the variation in radius of rotation as a function of gantry angle for ultra-high-resolution pinhole SPECT." *IEEE Trans. Nucl. Sci.*, vol. 52(5), pp. 1236-1242, 2005.

[4] M. Defrise C. Vanhove and J. Nuyts, "Perturbative refinement of the geometric calibration in pinhole SPECT." *IEEE Trans. Med. Imag.*, vol.27, pp. 204-214, 2008.

[5] D. Bequé, J. Nuyts, P. Suetens, and G. Bormans, "Optimization of geometrical calibration in pinhole SPECT." *IEEE Trans. Med. Imag.*, vol. 24(2), pp. 180-190, 2005.

[6] J. Nuyts, K. Vunckx, M. Defrise and C. Vanhove, "Small animal imaging with multi-pinhole SPECT." *Methods*, 48(2), pp. 83-91, 2009.

[7] K. Vunckx, J. Nuyts, B. Vanbilloen, M. De Saint-Hubert, D. Vanderghinste, D. Rattat, F. M. Mottaghy, and M. Defrise, "Optimized multipinhole design for mouse imaging." *IEEE Trans. Nucl. Sci.*, vol. 56(5), pp. 2696-2705, 2009.

[8] H. M. Hudson and R. S. Larkin, "Accelerated image reconstruction using ordered subsets of projection data." *IEEE Trans. Med. Imag.*, 13(4), pp. 601-609, 1994.